Distance Measurements by Dipolar Recoupling Two-Dimensional Solid-State NMR

S. Kiihne, M. A. Mehta, J. A. Stringer, D. M. Gregory,† J. C. Shiels,‡ and G. P. Drobny*

Departments of Chemistry and Physics, University of Washington, Seattle, Washington 98195

Received: July 2, 1997; In Final Form: December 11, 1997

We present a two-dimensional NMR technique for the measurement of dipolar couplings in polycrystalline solids. This experiment is fully transverse and uses a windowless dipolar recoupling pulse sequence (DRAWS, described in Gregory, D. M.; et al. *Chem. Phys. Lett.* **1995**, *246*, 654−663) to effect coherence transfer. Direct, internuclear coherence transfer produces negative cross-peaks in the 2D spectrum. Cross-peak development and experimental requirements for obtaining distances from the two-dimensional solid-state NMR spectra of two- and three-spin systems are discussed, and demonstrations are shown for thymidine-*2,4*-$^{13}C_2$ and L-alanine-$^{13}C_3$. Internuclear distances are derived by comparison of experimental cross-peak buildup curves with numerical simulations. In the three-spin system, indirect coherence-transfer mechanisms prohibit the interpretation of buildup curves as due to isolated spin pair interactions and limit the accuracy of some distance measurements. This 2D technique can also be used for spectral assignment, as demonstrated by an application to L-arginine·HCl-U-^{13}C,^{15}N.

Introduction

In dipolar recoupling pulse sequences, radio frequency pulses are applied during "magic angle spinning" (MAS) to avoid averaging the nuclear dipolar interaction, while simultaneously effecting near complete reduction of the chemical shift anisotropy (CSA). Numerous dipolar recoupling techniques have been reported in the literature,[1−12] and several have been incorporated into two-dimensional pulse sequences for spectral assignment.[3,11,13−17] Quantitative distance measurements using these techniques have generally been limited to a single spectral dimension in which a single distance between two rare spins on a sparsely labeled compound is measured.[18−20] Herein, we introduce a two-dimensional (2D) dipolar recoupling pulse sequence, 2D DRAWS, and demonstrate its applications for both spectral assignment and quantitative distance measurement. 2D DRAWS is a fully transverse experiment based on the one-dimensional technique, dipolar recoupling with a windowless sequence (DRAWS).[10]

Dipolar recoupling pulse sequences used for quantitative distance measurement must effect coherence transfers with more or less equal efficiency across the broad spectral bandwidth characteristic of ^{13}C spins in high-magnetic fields. The sequence should be relatively insensitive to the mutual orientations of the CSA tensors, and it should produce two-dimensional spectra with purely absorptive peaks.[21] The broad-band nature of DRAWS and its relative insensitivity to residual CSA effects[19] make it a promising candidate for a 2D dipolar recoupling distance measurement technique.

To measure distances with two-dimensional NMR pulse sequences, a series of two-dimensional spectra is acquired, each corresponding to a different mixing period. Internuclear distances are derived from plots of cross-peak volumes as a function of the duration of the mixing period. In high-resolution NMR, longitudinal magnetization is transferred between dipolar-coupled spins by cross-relaxation. In the simplest case of an isolated spin 1/2 pair, the rate of magnetization transfer is sensitive to the inverse sixth power of the internuclear distance. However, the nuclear Overhauser effect (NOE) is also sensitive to the overall tumbling rate of the molecule, the rates and amplitudes of internal molecular motions, and the direct coupling of individual sites to the lattice.[22] Indirect magnetization-transfer pathways may also complicate the quantitative analysis. Although extensive effort has been expended to quantify NOESY data, in the presence of these complicating factors, semiquantitative analysis in terms of distance ranges is often used.[23]

Two-dimensional solid-state dipolar recoupling experiments differ from NOESY experiments in several important respects. First, because they effect magnetization transfers with static dipolar couplings, the rate of coherence transfer is related to the inverse cube of the internuclear distance. Thus, other conditions being equal, solid-state dipolar recoupling experiments can measure longer distances than those measurable with NOESY experiments. Second, in most molecular solids, the amplitudes of molecular motions are somewhat smaller than those observed in liquids. The complicating effects of motional averaging can be further reduced by lowering the temperature. Unfortunately, the effects of indirect coherence transfers are of particular concern in the strongly coupled spin systems encountered in the solid state. We will show that, even at short mixing periods, cross-peak buildup curves for L-alanine-$^{13}C_3$ cannot be simulated by factoring the system into three, separate pairwise coherence-transfer problems. We will also show that, although numerical simulations involving the full spin network do reproduce the experimental results and allow quantitative distance measurements, in many cases longer distances in multispin systems cannot be determined with the same precision achievable in two-spin systems.

Finally, with an application to L-arginine·HCl-U-^{13}C,^{15}N, we demonstrate that spectral assignment is possible with the 2D DRAWS experiment. As in the MELODRAMA,[11] RIL-DQT,[14] and C7[17] experiments, which transfer magnetization by a double quantum mechanism, the 2D DRAWS experiment produces negative cross-peaks (relative to the diagonal "autocorrelation"

* To whom correspondence should be addressed.
† Present address: Chemistry Division Bldg. 200, Argonne National Laboratory, 9700 South Cass Ave., Argonne, IL 60439-4831.
‡ Present address: Department of Chemistry, Hall-Atwater Labs, Wesleyan University, Middletown, CT 06459.

S1089-5639(97)02141-5 CCC: $15.00
Published on Web 03/07/1998

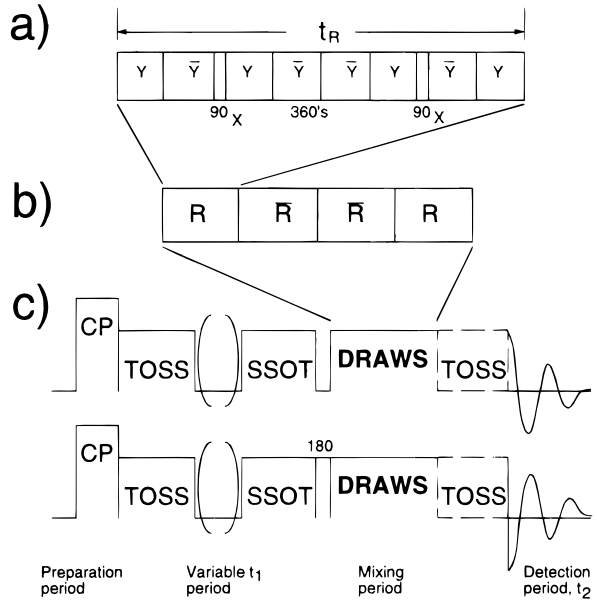

Figure 1. (a) Basic DRAWS pulse sequence, (b) the four rotor period supercycle, and (c) the full 2D sequence. Only the ^{13}C pulses are shown. The ^{1}H power is ramped during the cross polarization period, then increased to >2.5 times the ^{13}C power to avoid a Hartmann−Hahn match condition during the recoupling period. ^{1}H power is lowered slightly during the observation period to prevent probe arcing. The real and imaginary parts of the 2D matrix are obtained by adding the results of the two experiments. Sideband suppression is incorporated to remove MAS-induced phase twisting.

peaks) for direct internuclear coherence transfers. The cross-peak signs alternate with each additional spin involved in the transfer mechanism, allowing clear identification of nearest neighbor sites.

Theory

The basic DRAWS experiment consists of a four-rotor-period supercycle, as shown in Figure 1b and discussed in ref 10. This dipolar recoupling supercycle can be applied during the mixing period of a two-dimensional experiment, as shown in Figure 1c. This supercycle enables magnetization transfer, which is detected as cross-peaks in the two-dimensional Fourier transform of the two-dimensional time domain data set. The number of DRAWS supercycles applied during the mixing time is incremented in successive experiments to yield cross-peak buildup curves from which distance information is obtained.

When the double quantum dipolar Hamiltonian is the driving force for coherence transfer in two-dimensional dipolar recoupling experiments, cross-peak signs alternate with the number of spins involved in the transfer during the mixing time.[11,14] In 2D DRAWS, where the Hamiltonian consists of both zero and double quantum components, cross-peak sign alternation is also observed. The cross-peak signs and the experimental procedures required for the observation of pure absorptive line shapes in the 2D DRAWS spectrum are easily understood by considering the propagation of the density matrix.

During the evolution period t_1, the sample spinning greatly reduces the dipolar couplings, so to a good approximation we need only consider the chemical shift precession. During MAS the motion of the rotor induces a time dependence in the chemical shift which, upon Fourier transformation, appears as a manifold of sidebands spaced by the rotor frequency about the isotropic peak.[24] In 2D experiments, this anisotropic time dependence leads to phase twisting in the 2D matrix when the

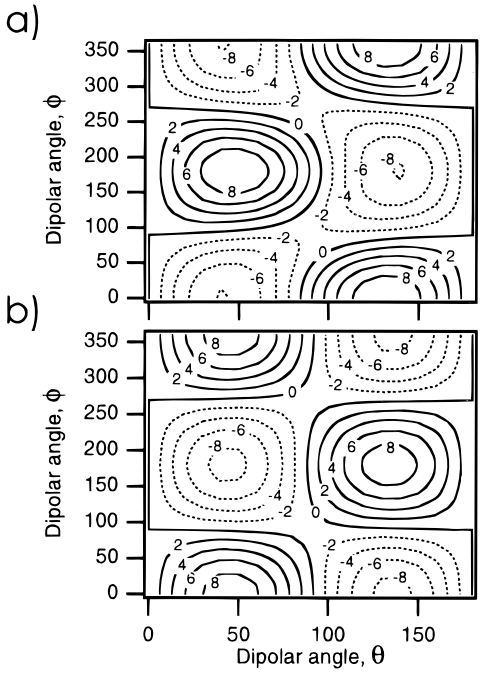

Figure 2. Orientation dependence of the DRAWS average Hamiltonian coefficients, c_{xx-yy} and c_{zz}. The angles θ, ϕ specify the orientation of the dipolar vector in the rotor frame. θ is the polar angle between the dipolar vector and the z-axis of the rotor frame, and ϕ is the azimuthal angle. The zero-quantum coefficient, c_{zz}, is shown in a, and the double-quantum coefficient, c_{xx-yy}, is shown in b.

rotor speed is slow relative to the CSA.[25] The removal of sidebands in the indirectly detected dimension simplifies the two-dimensional spectrum and allows the observation of pure phase peaks, as will be demonstrated below. For our immediate purposes, the application of TOSS[26−28] or SELTICS[29] renders the MAS chemical shift Hamiltonian time-independent during t_1. It then assumes the form

$$H_{CS} = -\Omega_1 I_{z1} - \Omega_2 I_{z2} \quad (1)$$

Assuming the initial density operator has the form $\rho(0) = I_{y1} + I_{y2}$ where I_{y1} is the operator representing the y component of the magnetization for spin 1 and I_{y2} is the corresponding operator for spin 2, the propagation of the density operator for a period of time, t_1, is easily obtained:

$$\begin{aligned}\rho(t) &= e^{-iHt_1}\rho(0)e^{iHt_1} \\ &= I_{y1}\cos\Omega_1 t_1 - I_{x1}\sin\Omega_1 t_1 + \\ &\qquad I_{y2}\cos\Omega_2 t_1 - I_{x2}\sin\Omega_2 t_1 \quad (2)\end{aligned}$$

where H is the time-independent Hamiltonian effective during the time t_1.

During the mixing period, dipolar recoupling is accomplished by the DRAWS pulse sequence. The time-independent, zeroth-order DRAWS Hamiltonian has been calculated previously as[10]

$$\bar{H}_D^{(0)} = \alpha(I_{x1}I_{x2} - I_{y1}I_{y2}) + \beta(3I_{z1}I_{z2} - I_1\cdot I_2) \quad (3)$$

where $\alpha = (d/17\pi)c_{xx-yy}$ and $\beta = (d/17\pi)c_{zz}$. The coefficients c_{xx-yy} and c_{zz} are given in ref 10, and d is the static dipolar coupling. This Hamiltonian is thus a mixture of double quantum (α) and zero quantum (β) terms. The effect of orientation on the coefficients is shown in Figure 2. Average Hamiltonian and Floquet calculations have also shown that, for the four rotor period supercycle shown in Figure 1a, the chemical shift offset and anisotropy effects are quite small.[10,30]

Thus, we neglect these effects during the mixing period and the density operator is assumed to evolve under the Hamiltonian given in eq 3:

$$\rho(t_1 + \tau) \approx e^{-i\bar{H}_D^{(0)}\tau}\rho(t_1)e^{i\bar{H}_D^{(0)}\tau} \quad (4)$$

No generality is lost, and the calculation is simplified if we consider only the terms that precess as Ω_1 during t_1. This is equivalent to considering only a single spin in the initial density matrix, I_{y1}. A straightforward calculation yields the expression

$$\begin{aligned}\rho(t_1 + \tau) = &\\ &\left[I_{y1}\cos\beta\tau\cos\left(\frac{\alpha-\beta}{2}\right)\tau + I_{y2}\sin\beta\tau\sin\left(\frac{\alpha-\beta}{2}\right)\tau\right]\cos\Omega_I t_1 - \\ 2&\left[I_{x1}I_{z2}\cos\beta\tau\sin\left(\frac{\alpha-\beta}{2}\right)\tau - I_{z1}I_{x2}\sin\beta\tau\cos\left(\frac{\alpha-\beta}{2}\right)\tau\right]\cos\Omega_I t_1 - \\ &\left[I_{x1}\cos\beta\tau\cos\left(\frac{\alpha+\beta}{2}\right)\tau - I_{x2}\sin\beta\tau\sin\left(\frac{\alpha+\beta}{2}\right)\tau\right]\sin\Omega_1 t_1 + \\ 2&\left[I_{y1}I_{z2}\cos\beta\tau\sin\left(\frac{\alpha+\beta}{2}\right)\tau + I_{z1}I_{y2}\sin\beta\tau\cos\left(\frac{\alpha+\beta}{2}\right)\tau\right]\sin\Omega_1 t_1\end{aligned} \quad (5)$$

There are eight terms in eq 5. The four linear terms indicate the observable components of the magnetization: the I_{x1} and I_{y1} terms are the autopeaks, while the I_{x2} and I_{y2} terms indicate the developing cross-peaks. The four bilinear terms (e.g. $I_{y1}I_{z2}$) represent antiphase magnetization.

It is clear from the I_{x2} and I_{y2} terms in eq 5 that the cross-peak sign develops during the mixing period and is a direct consequence of the commutation relations between the effective dipolar recoupling Hamiltonian and the spin state at the end of the t_1 period. In other two-dimensional solid-state NMR dipolar recoupling experiments,[11,14] the alternation of cross-peak sign in a network of coupled spins is attributed to the action of the double-quantum Hamiltonian when it dominates the coherence-transfer mechanism. In 2D DRAWS, the coherence-transfer mechanism is influenced by both the zero and the double-quantum parts of the DRAWS Hamiltonian, as indicated by the fact that the I_{x2} and I_{y2} terms in eq 5 precess at $\alpha + \beta$ and $\alpha - \beta$, respectively.

Propagation of the density matrix in t_2 clarifies the procedures required to observe pure absorpion line shapes in the 2D DRAWS spectrum. The calculation is simplified somewhat by considering only the observable components of the magnetization.

$$\begin{aligned}\rho^{obs}(t_1 + \tau + t_2) = &\\ &(I_{y1}\cos\Omega_1 t_2 - I_{x1}\sin\Omega_1 t_2)\cos\beta\tau\cos\left(\frac{\beta-\alpha}{2}\right)\tau\cos\Omega_1 t_1 - \\ &(I_{y2}\cos\Omega_2 t_2 - I_{x2}\sin\Omega_2 t_2)\sin\beta\tau\sin\left(\frac{\beta-\alpha}{2}\right)\tau\cos\Omega_1 t_1 + \\ &(I_{x1}\cos\Omega_1 t_2 + I_{y1}\sin\Omega_1 t_2)\cos\beta\tau\cos\left(\frac{\alpha+\beta}{2}\right)\tau\sin\Omega_1 t_1 - \\ &(I_{x2}\cos\Omega_2 t_2 + I_{y2}\sin\Omega_2 t_2)\sin\beta\tau\sin\left(\frac{\alpha+\beta}{2}\right)\tau\sin\Omega_1 t_1\end{aligned} \quad (6)$$

Equation 6 contains a mixture of cosine and sine terms in t_1. To obtain purely absorptive line shapes, these two components must be separated. There are several methods for doing this.[31] In general, a 180° pulse applied just before the mixing period changes the sign of the phase accumulated during t_1 leading to a technique known as "time reversal". In MAS experiments, the rotor motion induces an anisotropy which is not reversed by the pulse,[25] resulting in phase twisting. The phase twisting can generally be neglected at faster spin rates and/or lower magnetic field strengths, but if the spin rate is slow relative to the CSA and sidebands are not suppressed, pure phase peaks cannot be observed in 2D MAS experiments. For instance, at 500 MHz, we have observed significant phase twisting in amino acid carbonyl resonances with spin rates of up to 5 kHz in both 2D DRAWS and 2D RFDR experiments. To obtain pure absorptive line shapes in the two-dimensional spectrum, the anisotropy is removed from the indirectly detected dimension (t_1) by the application of a TOSS sequence[26−28] at the beginning of the t_1 period and a time-reversed TOSS sequence (i.e. SSOT) at the conclusion of the t_1 period, just before the mixing period.[32,33] Selective elimination of chemical shift (SELTICS)[29] has been used successfully as well. This TOSS−SSOT couple applied during the t_1 period effectively removes the chemical shift anisotropy, allowing the observation of pure phase peaks and the use of a 180° pulse for time reversal (see Figure 6).

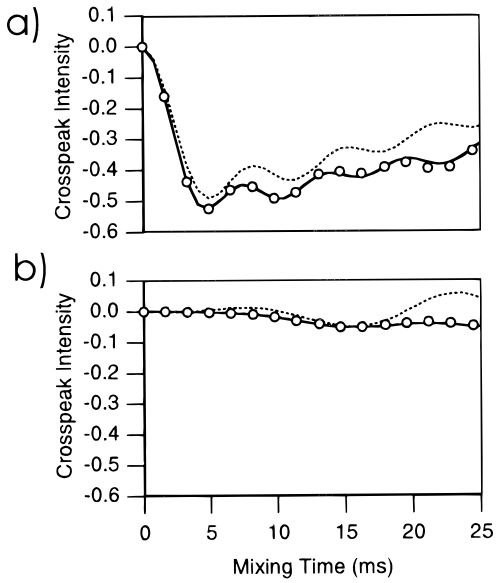

Figure 3. Rates of cross-peak development for different initial conditions. In a, the initial condition is I_{y1}, and the trace of I_{y2} with the density matrix is shown as a function of the mixing period, corresponding to the $\alpha-\beta$ terms in eqs 6 and 7. The curve marked by open circles was derived using the average Hamiltonian given in eq 3. This simulation is compared to numerical calculations where CSA effects have either been omitted (solid line) or included (dotted line). In b, the initial condition is I_{x1}, and the trace of I_{x2} with the density matrix is shown. This corresponds to the $\alpha + \beta$ terms in eqs 6 and 7. As above, the average Hamiltonian calculation is represented by open circles and is compared to numerical calculations where CSA effects have been omitted (solid line) and included (dotted line). The chemical shift parameters are those published previously for thymidine-*4,6*-$^{13}C_2$.[10] In the numerical simulations, the DRAWS sequence was applied with $90°_y$ pulses. Each curve is an averge over 500 crystallites.

If a time-reversing, 180° pulse is applied, the observable signal in t_2 is

$$\begin{aligned}\rho_{180}^{obs}(t_1 + \tau + t_2) = &\\ &(I_{y1}\cos\Omega_1 t_2 - I_{x1}\sin\Omega_1 t_2)\cos\beta\tau\cos\left(\frac{\beta-\alpha}{2}\right)\tau\cos\Omega_1 t_1 - \\ &(I_{y2}\cos\Omega_2 t_2 - I_{x2}\sin\Omega_2 t_2)\sin\beta\tau\sin\left(\frac{\beta-\alpha}{2}\right)\tau\cos\Omega_1 t_1 - \\ &(I_{x1}\cos\Omega_1 t_2 + I_{y1}\sin\Omega_1 t_2)\cos\beta\tau\cos\left(\frac{\alpha+\beta}{2}\right)\tau\sin\Omega_1 t_1 + \\ &(I_{x2}\cos\Omega_2 t_2 + I_{y2}\sin\Omega_2 t_2)\sin\beta\tau\sin\left(\frac{\alpha+\beta}{2}\right)\tau\sin\Omega_1 t_1\end{aligned} \quad (7)$$

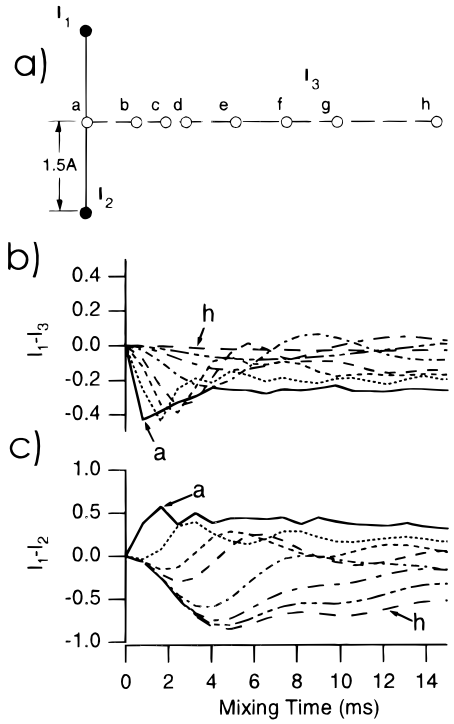

Figure 4. Effects of spin geometry and indirect coherence-transfer pathways on 2D DRAWS cross-peak buildup rates. The geometries shown in a were used to calculate the curves shown in b and c. Calculations included the chemical shift, RF, and pairwise dipolar interactions between spins I_1, I_2, and I_3 and were carried out by considering an initial spin state I_{y1} and taking the trace of the density matrix with the observable I_{y2} after a given mixing time. Chemical shift parameters were those of L-alanine where I_1 = CO, I_2 = Cα, and I_3 = Cβ. (b) The I_1-I_3 DRAWS cross-peak buildup curves calculated for the geometries shown in a. The I_1-I_3 distances are 1.5, 2.0, 2.3, 2.5, 3.0, 3.5, 4.0, and 5.0 Å in a through h, respectively. (c) I_1-I_2 DRAWS cross-peak buildup curves calculated for the geometries shown in a. The internuclear distance is held constant at 3 Å. Each curve is an average over 500 randomly oriented crystallites.

In principle, the two signals described by eqs 6 and 7 can be combined in either of two ways. Addition of the two signals causes cancellation of the terms containing sin $\Omega_1 t_1$. This leads to a cosine modulated signal, the real part of a matrix with negative cross-peaks which are formed at a rate $\alpha - \beta$. Subtraction of the two signals cancels the cos $\Omega_1 t_1$ terms, yielding the imaginary part of a matrix with positive cross-peaks which build up at a rate $\alpha + \beta$. As shown in Figure 2, for any given orientation, α and β are similar in magnitude but opposite in sign. This results in very different rates of cross-peak development, as shown in Figure 3. In practice, only the $\alpha - \beta$ terms result in significant cross-peak intensities.

A phase-sensitive two-dimensional spectrum is obtained by performing a second experiment with the DRAWS irradiation shifted in phase by 90°. This effectively changes the sign of the double-quantum term in eq 3. When applied to an initial density operator I_{y1}, the sign of α in eqs 6 and 7 changes. When subtracted from the corresponding time-reversed data set, quadrature data in t_1 are obtained. Hypercomplex Fourier transformation[34,35] of the resulting data yields a two-dimensional DRAWS spectrum in which all auto- and cross-peaks are purely absorptive.

Although the alternation of cross-peak sign enables the unambiguous determination of internuclear connectivities, in multispin systems it may also complicate the derivation of quantitative distance information from two-dimensional data. To study the conditions that determine cross-peak signs and to

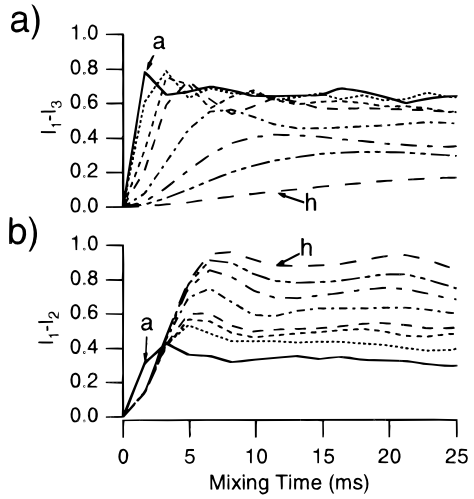

Figure 5. Effects of spin geometry and indirect coherence-transfer pathways on 2D RFDR cross-peak buildup rates. The geometries shown in Figure 4a were used to calculate the curves shown in a and b. Calculations included the chemical shift, RF, and pairwise dipolar interactions between spins I_1, I_2, and I_3. Chemical shift parameters were those of L-alanine where I_1 = CO, I_2 = Cα, and I_3 = Cβ. The calculations were carried out as described in Figure 4. (a) I_1-I_3 RFDR cross-peak buildup curves calculated for the geometries shown in 4a. The I_1-I_3 distances are 1.5, 2.0, 2.3, 2.5, 3.0, 3.5, 4.0, and 5.0 Å in a through h, respectively. (b) I_1-I_2 RFDR cross-peak buildup curves calculated for the geometries shown in 4a. The internuclear distance is held constant at 3 Å.

quantify the effects of indirect magnetization-transfer mechanisms, we have simulated the effects of applying the DRAWS pulse sequence to a series of three-spin geometries, shown in Figure 4a. The initial magnetization was I_{y1}, and the buildup of magnetization components I_{y2} and I_{y3} was followed as a function of the mixing time. A series of these buildup curves for I_{y3} are shown in Figure 4b. At short mixing times, the I_1-I_3 cross-peaks are negative in all of these geometries, indicating direct internuclear coherence transfer between spins 1 and 3. Both the cross-peak buildup rate and the relative cross-peak intensity appear to be related to the internuclear distance; however, at longer mixing times, some cross-peaks actually change sign, some geometries lead to the formation of only relatively small cross-peaks (e.g. conformation e, where all distances are 3 Å), and all the cross-peaks are attenuated relative to the two spin system. Hence, the best indicator of internuclear distance appears to be the initial buildup rate. This conclusion is further supported by the buildup curves shown in Figure 4c for the I_{y2} magnetization. This represents the I_1-I_2 cross-peak buildup in the presence of the third spin, where the I_1-I_2 distance is held constant at 3 Å. When the third spin is over 4 Å away, the curve closely resembles the 1D DRAWS decay curve; however, as the distance to the third spin decreases, the I_1-I_2 cross-peak intensity decreases. When all the distances are equal (conformation e), the cross-peak formed is relatively small, and it changes sign at longer mixing times. When the third spin lies between the other two (conformations a−d), a positive cross-peak is formed, and its buildup rate, even at short mixing times, does not reflect the actual internuclear distance. It is clear that, as long as the observed 2D DRAWS cross-peaks are negative, the buildup rate at short mixing times is the best indication of the internuclear distance.

It is interesting to compare these results for the 2D DRAWS sequence with those from 2D radio frequency dipolar recoupling (RFDR).[3] Since the cross-peaks observed in the DRAWS experiment are due to a mixed double- and zero-quantum

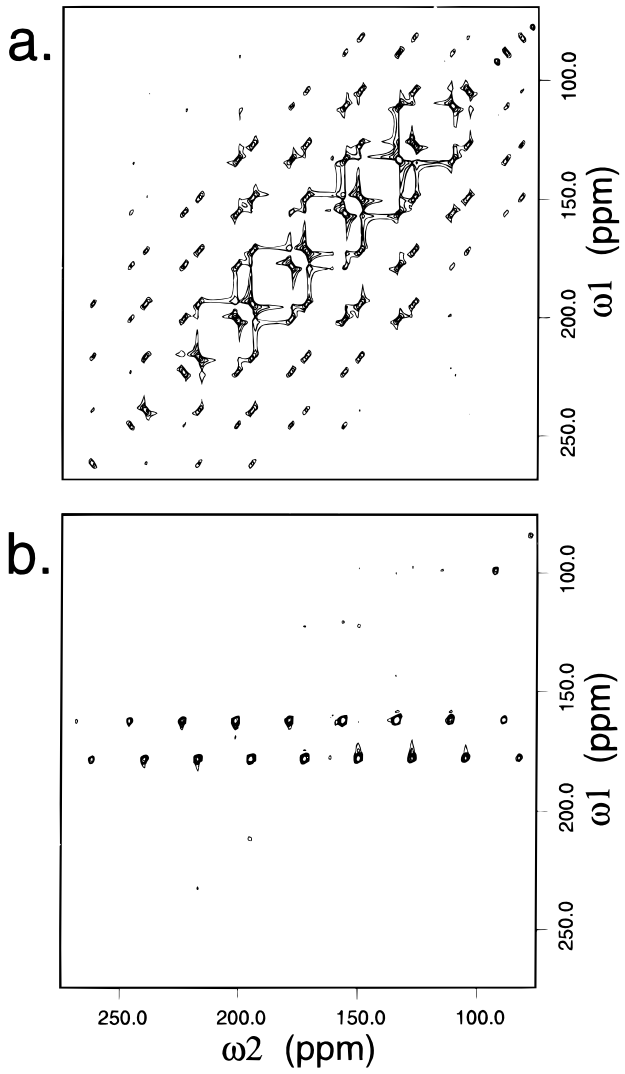

Figure 6. Effects of MAS on phase in time reversal experiments for thymidine-*2,4*-$^{13}C_2$. The matrix in a) was collected using time reversal without sideband suppression. A 180° pulse was used to reverse the sense of precession after the t_1 period. This was added to the result of the unreversed experiment to yield the real part for the Fourier transform. Subtraction yielded the imaginary part. In b, TOSS−SSOT was incorporated in the t_1 period. Phase cycling and processing remained unchanged. The spin rate was 2 kHz.

Hamiltonian, the sum magnetization of the system is not conserved, and the cross-peaks due to different mechanisms interfere, leading to a reduction of the cross-peak signal intensity. In 2D RFDR, cross-peaks are formed by an effective zero quantum Hamiltonian, and the sum magnetization of the system is conserved.[3] The effects of indirect magnetization transfer on 2D RFDR buildup curves are shown in Figure 5. These buildup curves are for the same geometries shown in Figure 4a and can be compared directly with parts b and c of Figure 4, respectively. In Figure 5a, the internuclear distance is varied, and the buildup curves show variations in both the initial buildup rate and the maximum cross-peak signal intensity. In Figure 5b, the internuclear distance is constant at 3 Å, and the initial buildup rate remains nearly constant, with the exception of the linear spin system geometry (conformation a). The maximum cross-peak intensity, however, does not remain constant. It is clear that, except in the case of a linear system, the initial slope of the cross-peak buildup curve is a reasonable indicator of the internuclear distance, while the cross-peak intensity is not. The total magnetization of the system is conserved in 2D RFDR; however, its distribution among the interacting resonances is determined by the distribution of dipolar couplings. Thus, irrespective of the method used to study the system, the intensity of a particular cross-peak reflects a distribution of distances, while the initial buildup rate more closely reflects the distance between the two interacting nuclei.

Experimental Section

Homonuclear 2D DRAWS correlation experiments were carried out on a home-built spectrometer operating at a ^{13}C Larmor frequency of 100.57 MHz. A triply tuned ^{1}H-$^{15}N-X$ probe from Doty scientific with a 5-mm spinner assembly was used for all the experiments. Spin rates were controlled to within ±5 Hz with a home-built spin rate controller.[36] The ^{13}C rf power levels were matched to the $t_r = 17\pi/2$ condition for the DRAWS experiment. The ^{1}H power levels were adjusted to 50 kHz during cross polarization and were increased to 115 kHz for CW decoupling during the evolution, mixing, and detection periods. The ^{1}H pulses were provided by a Henry Radio 2004-A amplifier, while the ^{13}C pulses were provided by a Kalmus LP-1000 amplifier. A 2-ms cross polarization period was used. Power levels were set and phase transients minimized using the method of Burum et al.[37] on $^{13}CCl_4$ (Cambridge Isotope Labs Inc.). Sidebands were suppressed either with the TOSS sequence of Raleigh et al.[38] or with SELTICS-8.[29] The 2D DRAWS cross-peak buildup studies were carried out at a rotor speed of 4.9 kHz with a ^{13}C power level of 41.6 kHz. In general, 512 transients were collected, multiplied with a shifted sine square apodization (90°), and zero filled to a matrix size of 1024 × 1024. The 2D simulations consisted of only 256 transients, but spin rates, pulse lengths, and processing were identical with those applied to the experimental data. Chemical shift and molecular parameters for the simulations are determined from refs 30 and 39−41. The cross-peak volumes were normalized to the sum of the diagonal peak volumes.

The phase of the initial ^{1}H pulse for cross polarization was inverted between successive experiments in order to suppress zero frequency peaks in the t_1 dimension of the final 2D matrix. When combined with "cyclops"[42] phase cycling, this led to a simple, eight-step phase cycle. To obtain pure phase spectra from these phase-modulated experiments, four experiments were combined. The first two utilize the same basic phase for all periods. In the second one, a 180° pulse is applied just before the DRAWS sequence to reverse the sense of the t_1 precession. These two experiments are added to yield the real part of the FID for the ω_1 dimension. In the second pair of experiments, the 180° pulse and the DRAWS sequence are both shifted by 90° relative to the preparation and the receiver. This pair of experiments is combined to yield the imaginary part of the indirectly detected FID.

L-Alanine-$^{13}C_3$ was obtained from Isotec, Inc., and cut to 10% with unlabeled material to minimize intermolecular dipolar interactions. The resultant mixture was lyophilized to dryness. The L-arginine·HCl-U-^{13}C,^{15}N was obtained from Cambridge Isotope Labs and used without dilution or further purification. The doubly labeled thymidine-*2,4*-$^{13}C_2$ was synthesized as reported earlier[10] and used neat.

Results

Consider a simplified 2D MAS experiment which omits TOSS−SSOT but uses time reversal for phase-sensitive detection. The 180° pulse applied at the beginning of the acquisition time falls at different rotor orientations after different t_1 periods.

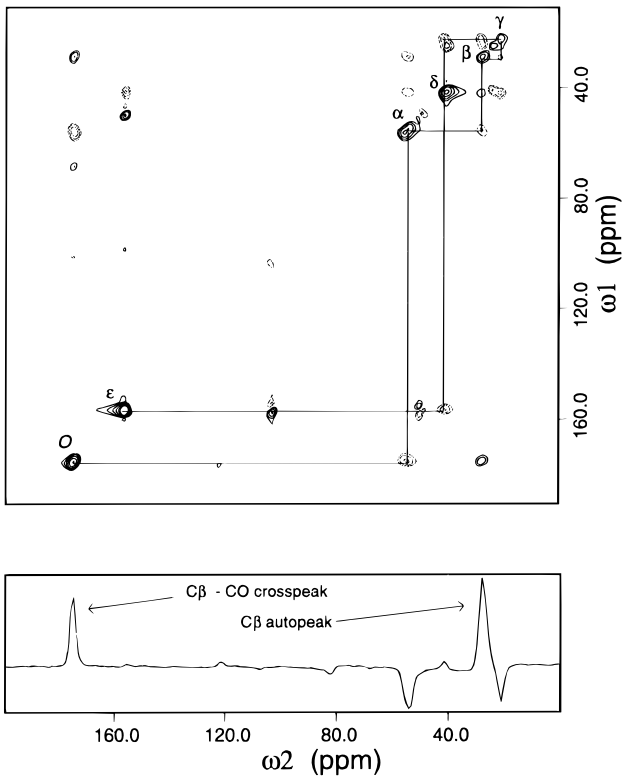

Figure 7. Two-dimensional chemical shift correlation spectrum for uniformly labeled L-arginine·HCl-$^{13}C,^{15}N$ and a single slice of the spectrum containing the Cβ autopeak. The mixing period was four rotor cycles at a spin rate of 5.35 kHz (0.748 ms). The ^{13}C power was 45.5 kHz, and the ^{1}H decoupling was raised to 115 kHz during DRAWS. Direct (two-spin) magnetization transfer leads to negative cross-peaks as seen in the Cβ slice at the bottom. The positive, Cβ−CO peak forms via an indirect (three-spin) magnetization-transfer mechanism.

While this pulse changes the sign of the phase acquired during t_1, it is not equivalent to time reversal. This interaction of the rotor motion with the experimental parameters leads to the phase twisting apparent in Figure 6a, which shows the result of this simplified experiment applied to [*2,4*-$^{13}C_2$]thymidine at a spin rate of 2 kHz. Figure 6b shows that this phase twisting is removed, and the result significantly simplified, by the application of the TOSS−SSOT sequence during the t_1 period. The matrix in Figure 6b is the result of a fully transverse, pure phase version of Kolbert and Griffin's original sideband separation experiment.[32] The magnitude of the phase twisting decreases with increasing spin rate, but similar effects have been observed at 4 kHz. To obtain truly pure phase spectra for quantitative distance measurements, we have used sideband suppression in the t_1 dimension of all 2D DRAWS experiments.

We have applied the 2D DRAWS experiment of Figure 1c to several relatively complex molecules to determine spin−spin connectivities for spectral assignment. Figure 7 shows an application of 2D DRAWS to L-arginine·HCl-U-$^{13}C,^{15}N$. The mixing time was 0.748 ms, leading to the observation of direct, nearest neighbor connections. The intensities of the cross-peaks are variable due to relaxation effects, but all the cross-peaks are visible, and the peak assignment can be made easily as shown. The matrix is quite simple, with small imperfections from the SELTICS sequences used to suppress sidebands in the t_1 dimension. The peaks are all purely absorptive, even to very low contour levels, and the cross-peaks are observed consistently over the very broad spectral width. At longer mixing times, positive cross-peaks appear between next-nearest-neighbor sites. Even at this short mixing period, the C0−Cβ cross-peak is positive, as seen in the slice at the bottom of Figure 7. The positive cross-peak sign indicates that this peak is not the result of a simple two-spin interaction, but involves indirect transfer of magnetization. Similar peaks are observed between other two-bond distances (e.g., Cα−Cγ, Cβ−Cδ), although the intensities are significantly smaller.

To use the 2D DRAWS experiment for distance measurement, we first considered the effects of combining TOSS with the 1D DRAWS experiment. Four experiments were applied to [2,4-$^{13}C_2$]thymidine. These incorporated TOSS, TOSS−SSOT, or both, as they are used in the t_1 and t_2 periods of the 2D DRAWS experiment. The number of applications of the DRAWS supercycle was incremented to yield DRAWS decay curves for each of the experiments. The resultant curves were indistinguishable from the decay curve obtained without TOSS, and simulations matched the data closely. Thus, distances obtained from either 1D or 2D DRAWS experiments are not compromised by sideband suppression.

The 2D DRAWS cross-peak buildup curve for thymidine-*2,4*-$^{13}C_2$ is shown in Figure 8. In these 2D experiments, successive time points are acquired by incrementing the number of DRAWS supercycles applied during the mixing time. A full 2D matrix is acquired at each time point. The peak volumes are measured using standard routines, and cross-peak volumes are normalized to the sum of the diagonal (auto) peaks. Also presented in Figure 8b is the simulation of the 2D buildup curve. For each time point in the buildup curve, the full 2D matrix was simulated, transformed, and corrected using the same techniques used to treat the experimental data. Each simulation calculated 500 randomly distributed crystallites using chemical shift and dipolar parameters published previously.[19]

The time behavior of the 2D cross-peak volumes is quite similar to that of the 1D DRAWS decay curves. On the basis of this similarity, it should be feasible to measure buildup curves for complex molecules and simulate the results directly if the system is separable into a series of isolated two-spin interactions. Unfortunately, this approximation is not appropriate. In general, indirect coherence transfer pathways are an important determinant of cross-peak volumes in multispin systems.

The effects of indirect coherence transfer mechanisms are clearly visible in Figure 9, which shows the results of a 2D DRAWS buildup experiment on L-alanine-$^{13}C_3$. The molecule contains three sites with internuclear distances as shown in Figure 9a. While the 1.5 Å distances develop negative cross-peaks in the 2D experiment as shown in Figure 9b,c, the longer 2.5 Å distance is characterized by a positive cross-peak as shown in Figure 9d. This sign change indicates that the longer distance, CO−Cβ cross-peak is dominated by an indirect transfer mechanism via the two shorter distances, CO−Cα and Cα−Cβ. In comparing these results with simulations of three separate two-spin systems, the maximum cross-peak intensity is attenuated, and the CO−Cβ cross-peak builds up relatively rapidly and its sign is inverted. These results indicate that the two-spin approximation commonly used in solution-state NMR experiments is not appropriate in analysis of these solid-state results.

The relative importance of other terms in the Hamiltonian can be seen in the other simulations shown. The spin−spin couplings (*J*-couplings) between neighboring carbons are relatively large in this system (55 Hz for C0−Cα and 35 Hz for Cα−Cβ),[41] and their effect is clearly seen in comparison with simulations that neglect these interactions. Interference between magnetization-transfer mechanisms due to dipolar and *J*-couplings causes a rapid decay of the negative cross-peak

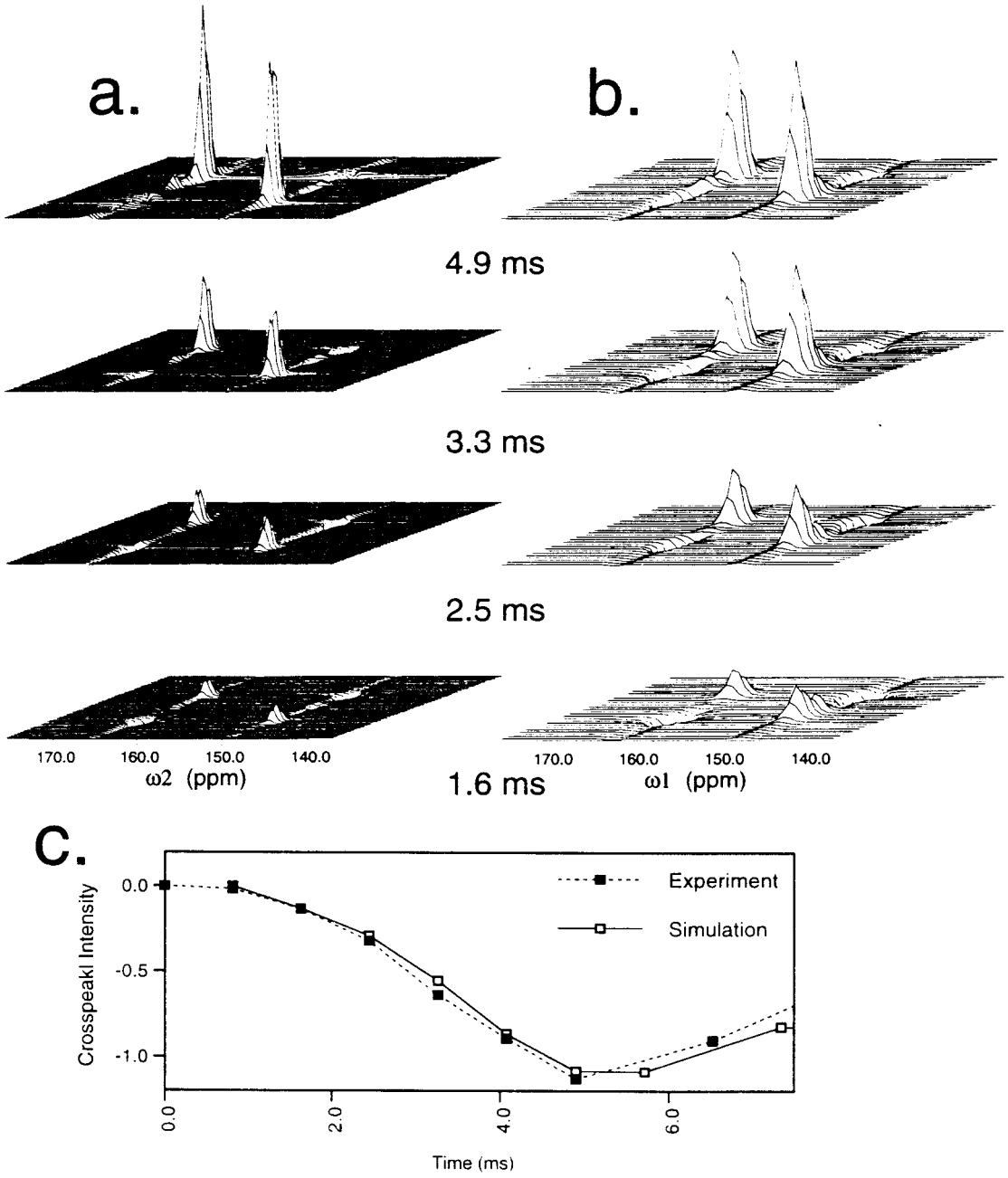

Figure 8. (a) Inverted experimental 2D DRAWS spectra of thymidine-*2,4*-$^{13}C_2$. (b) Inverted 2D simulations of the experimental data. Only 256 transients were simulated, leading to the reduction in resolution compared to the experiment. (c) Comparison of experimental and simulated cross-peak volumes.

intensity associated with the two short internuclear distances, as shown by the dotted lines in the figure. The initial buildup rates are unaffected, as is the positive cross-peak associated with the longer distance interaction. Since this cross-peak is primarily due to indirect dipolar coherence transfer, the relative importance of the direct dipolar coupling between CO and Cβ gives some indication of the accuracy to which this longer distance can be determined experimentally. Unfortunately, this coupling does not significantly change the buildup curves (dashed lines). Thus, even when indirect pathways are considered in the calculations, there are severe limits on the quantitative interpretation of cross-peak intensities and buildup curves in terms of internuclear distances, particularly for positive cross-peaks whose development is dominated by indirect pathways.

Discussion

A prerequisite of distance determinations is the assignment of the observed spectral peaks to particular nuclei in the molecule under investigation. The 2D DRAWS experiment can be used for such studies, as indicated by the application to uniformly ^{13}C-labeled L-arginine. This assignment technique is quite similar to the correlation spectroscopy method of Geen et al.;[17] however, the observed cross-peaks are significant relative to the autopeaks, obviating the need for double-quantum filtering in this uniformly labeled system. Double-quantum filtering can be accomplished with the DRAWS technique and may prove of use for samples with large natural abundance background signals such as randomly labeled biomolecules.[43] The usefulness of double-quantum filtering techniques is limited by signal losses through the double-quantum filter, and such

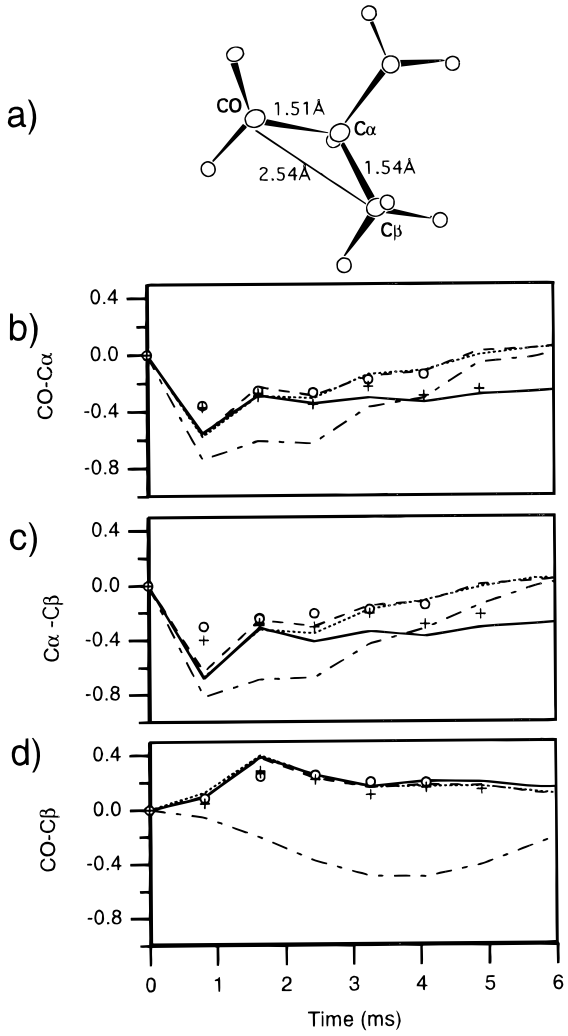

Figure 9. (a) L-Alanine-$^{13}C_3$ structure and distances used in simulations.[47−49] Graphs b, c, and d contain comparisons of experimental cross-peak buildup curves (○) with simulations based on different approximations to the full spin system for the CO−Cα, Cα−Cβ, and CO−Cβ cross-peaks, respectively. A full 2D simulation, neglecting *J*-couplings, is shown by (+) marks. All lines represent 1D simulations (see Figure 4). The solid line neglects the *J*-couplings, showing the correspondence between the two simulation methods. The dotted line (···) shows the effect of including *J*-couplings, and the dashed line (- - -) shows the effect of neglecting the direct CO−Cβ dipolar coupling completely. The dashed−dotted line (− · −) corresponds to simulations of separate two-spin systems for each dipolar spin pair interaction.

methods are not expected to be the primary weapons in the armamentarium for study of uniformly labeled molecules. A correlation method that relies on spin−spin couplings to effect coherence transfer has been proposed by Baldus et al.,[44,45] who suggest the name TOBSY (through bond spectroscopy). In this technique, dipolar couplings and chemical shift effects are eliminated during the mixing period by high-power windowless RF irradiation to yield a Hamiltonian that is directly analogous to the TOCSY experiment of solution state NMR. As in liquids, each of these spectral assignment techniques is expected to be useful under particular experimental and sample conditions.

It is interesting to consider the degree to which factors complicating the structural interpretation of 2D DRAWS data are common to other NMR methods for structure determination, particularly two-dimensional NOE spectroscopy (NOESY). Unlike 2D DRAWS and other solid-state dipolar recoupling pulse sequences that transfer coherence, NOESY experiments involve transfers of longitudinal magnetization. Like 2D DRAWS, the structural interpretation of NOESY data is often complicated when magnetization is transferred through indirect pathways. Although it has long been recognized that only the initial magnetization buildup curves can be reliably used for measurements of internuclear distances,[46] it is also clear that unfavorable structural conditions can make it difficult to interpret these data.

In NOESY experiments, the integrated intensity of the cross peak between two spins *k* and *l* following a mixing period of length τ_M is given by[21]

$$I_{jk}(\tau_M) = I_{kj}(\tau_M) = -\frac{M_0}{2}\frac{W^{kl}{}_2 - W^{kl}{}_0}{W^{kl}{}_2 - W^{kl}{}_0}[1 - \exp(-\tau_M R_C)]e^{-R_L\tau_M} \quad (8)$$

where W_0 and W_2 are the zero-quantum and double-quantum transition probabilities, respectively, R_C is the cross relaxation rate, which is defined as $R_C = 2|W_2^{kl} - W_0^{kl}|$, and R_L is the rate of energy transfer from the spin system directly to the lattice (i.e., the leakage rate). The relative magnitudes of the transition probabilities W_0 and W_2 are dependent on the rate of the dynamic process that gives rise to the NOE. Thus, the cross-peak signs in NOESY experiments depend on the rates of the motions that give rise to the NOE. This is in contrast to 2D DRAWS, in which cross-peak signs are a result of the dominant coherence-transfer pathway.

Assuming two spins *k* and *l* are separated by a number of intervening spins *j*, the *k*−*l* NOESY cross-peak amplitude can be expanded in powers of the product of the mixing time and elements of the cross relaxation matrix. For short mixing times τ_M, this leads to

$$I_{kl}(\tau_M) \propto R_{kl}\tau_M + \frac{1}{2}\sum_j R_{kj}R_{jl}\tau_M^2 + ... \quad (9)$$

where R_{kl} is the rate of direct magnetization transfer between spins *k* and *l*, and R_{kj} and R_{jl} are magnetization-transfer rates from spins *k* and *l* to an intervening spin *j*. If the direct rate R_{kl} is dominant, the initial NOE buildup curve is linear and can in principle be used to deduce internuclear distance. If R_{kl} is small compared to second-order terms, the initial buildup curve has a quadratic form, and accurate determination of the distance between spins *k* and *l* is not possible. In practice, determination of the magnetization-transfer mechanism from initial NOESY buildup curves is difficult if sensitivity is low.

Similar effects control the development of cross-peaks in 2D solid-state dipolar recoupling experiments, limiting the interpretation of distances from cross-peaks whose buildup curves are dominated by indirect coherence-transfer mechanisms. In 2D DRAWS and double-quantum transfer experiments, such indirect cross-peaks are easily discerned by considering the sign of the cross-peak. In 2D RFDR and other zero-quantum transfer experiments, such cross-peaks are not readily identified, and the situation is closer to that found in liquids where the effects of indirect coherence-transfer mechanisms are often difficult to determine. In either case, it is clear that even if the Louivillian formulation of the solid-state experiment can be reduced to a liquidlike rate matrix, a two-spin approximation is not warranted. In this work, we have considered only direct simulation of the full spin system as a method of distance determination. While this method is not applicable to much larger spin systems, it does allow analysis of the limitations of these experiments for distance measurements in multispin systems.

Conclusion

We have shown that well-resolved, easily assigned two-dimensional spectra can be obtained with a pulse sequence that uses a DRAWS irradiation for dipolar recoupling during the mixing period. Applications to thymidine-*2,4*-^{13}C have shown that well-resolved, pure absorption phase spectra can be obtained when spinning sidebands are removed from the t_1 dimension. It has been shown that the removal of sidebands does not affect 1D DRAWS distance measurements and that the time behavior of cross-peaks in the 2D experiment is closely analogous to the 1D decays used to measure distances. This should allow the 2D method to have the same broad applicability demonstrated earlier for the 1D DRAWS experiment: insensitivity to chemical shift parameters, pulse imperfections, and RF inhomogeneity. We have shown that both positive and negative cross-peaks can be selected by judicious use of time reversal, and by using average Hamiltonian theory to propagate the density matrix, we demonstrate that the development of the relative cross-peak sign is a function of the form of the Hamiltonian effective during the mixing period. We have demonstrated that internuclear distances can be measured in multispin systems by simulation of cross-peak volume buildup curves if the 2D DRAWS cross-peak is negative relative to the autopeak. Even in this favorable case, indirect coherence-transfer mechanisms are an important factor in cross-peak buildup rates and must be considered in any distance determination from a 2D DRAWS experiment, but both experiments and simulations support the use of buildup curves at short mixing times to determine internuclear distances from negative cross-peaks. Applications of 2D DRAWS to uniformly labeled biomolecules are in progress, along with further investigations of the applicability and limitations of this technique for internuclear distance measurements.

Acknowledgment. G.D. acknowledges support from NIH Grant ROIGM47802-03 and from NIH Program Project Grant GM32681-14. J.A.S. acknowledges support from NIH Tranining Grant GM08268.

References and Notes

(1) Tycko, R.; Dabbagh, G. *Chem. Phys. Lett.* **1990**, *173*, 461−5.
(2) Gullion, T.; Vega, S. *Chem. Phys. Lett.* **1992**, *194*, 423−428.
(3) Bennett, A. E.; Ok, J. H.; Vega, S.; Griffin, R. G. *J. Chem. Phys.* **1992**, *96*, 8624.
(4) Sodickson, D. K.; Levitt, M. H.; Vega, S.; Griffin, R. G. *J. Chem. Phys.* **1993**, *98*, 6742−6748.
(5) Fujiwara, T.; Ramamoorthy, A.; Nagayama, K.; Hioka, K.; Fujito, T. *Chem. Phys. Lett.* **1993**, *212*, 81−84.
(6) Joers, J. M.; Rosanske, R.; Gullion, T.; Garbow, J. R. *J. Magn. Reson., Ser. A* **1994**, *106*, 123−126.
(7) Klug, C. A.; Zhu, W.; Merrit, M. E.; Schaefer, J. *J. Magn. Reson., Ser. A* **1994**, *109*, 134−136.
(8) Nielsen, N. C.; Bildsoe, H.; Jakobsen, H. J.; Levitt, M. H. *J. Chem. Phys.* **1994**, *101*, 1805−1812.
(9) Lee, Y. K.; Kurur, N. D.; Helmle, M.; Johannessen, O. G.; Nielsen, N. C.; Levitt, M. H. *Chem. Phys. Lett.* **1995**, *242*, 304−309.
(10) Gregory, D. M.; Mitchell, D.; Stringer, J. A.; Kiihne, S. R.; Shiels, J. C.; Callahan, J.; Mehta, M. A.; Drobny, G. P. *Chem. Phys. Lett.* **1995**, *246*, 654−663.
(11) Sun, B.-Q.; Costa, P. R.; Kocisko, D.; Lansbury, P. T., Jr.; Griffin, R. G. *J. Chem. Phys.* **1995**, *102*, 702−707.
(12) Gottwald, J.; Demco, D. E.; Graf, R.; Spiess, H. W. *Chem. Phys. Let.* **1995**, *243*, 314−323.
(13) Weintraub, O.; Vega, S.; Hoelger, C.; Limbach, H. H. *J. Magn. Reson., Ser. A* **1994**, *109*, 14−25.
(14) Baldus, M.; Tomaselli, M.; Meier, B. H.; Ernst, R. R. *Chem. Phys. Lett.* **1994**, *230*, 329−336.
(15) Griffiths, J. M.; Laksmi, K. V.; Bennett, A. E.; Raap, J.; Van der Vielen, C. M.; Lugtenburg, J.; Herzfeld, J.; Griffin, R. G. *J. Am. Chem. Soc.* **1994**, *116*, 10178−10181.
(16) Fujiwara, T.; Sugase, K.; Kainosho, M.; Ono, A.; Ono, A.; Akutsu, H. *J. Am. Chem. Soc.* **1995**, *117*, 11351−11352.
(17) Geen, H.; Gottwald, J.; Graf, R.; Schnell, I.; Spiess, H. W.; Titman, J. J. *J. Magn. Reson., Ser. A* **1997**, *125*, 224−227.
(18) Griffiths, J. M.; Ashburn, T. T.; Auger, M.; Costa, P. R.; Griffin, R. G.; Lansbury, P. T. J. *J. Am. Chem. Soc.* **1995**, *117*, 3539−46.
(19) Mehta, M. A.; Gregory, D. M.; Kiihne, S. R.; Mitchell, D. J.; Hatcher, M. E.; Shiels, J. C.; Drobny, G. P. *Solid State NMR* **1996**, *7*, 211−228.
(20) Peersen, O. B.; Smith, S. O. *Concepts Magn. Reson.* **1993**, *5*, 303−317.
(21) Ernst, R. R.; Bodenhausen, G.; Wokaun, A. *Principles of Nuclear Magnetic Resonance in One and Two Dimensions*; Clarendon Press: Oxford, 1987; p 610.
(22) Keepers, J. W.; James, T. L. *J. Magn. Reson* **1984**, *57*, 404−426.
(23) Wüthrich, K. *NMR of Proteins and Nucleic Acids*; John Wiley and Sons: New York, 1986; p 292.
(24) Herzfeld, J.; Berger, A. E. *J. Chem. Phys.* **1980**, *73*, 6021−6030.
(25) Schmidt-Rohr, K.; Spiess, H. W. *Multidimensional Solid-state NMR and Polymers*; Academic Press: Harcourt Brace and Co.: London, 1994; p 478.
(26) Dixon, W. T. *J. Chem. Phys.* **1982**, *77*, 1800−1809.
(27) Raleigh, D. P.; Olejniczak, E. T.; Vega, S.; Griffin, R. G. *J. Magn. Reson.* **1987**, *72*, 238−250.
(28) Antzutkin, O. N.; Song, Z.; Feng, X.; Levitt, M. H. *J. Chem. Phys.* **1994**, *100*, 130−140.
(29) Hong, J.; Harbison, G. S. *J. Magn. Reson. A* **1993**, *105*, 128−136.
(30) Gregory, D. M.; Mehta, M. A.; Shiels, J. C.; Drobny, G. P. *J. Chem. Phys.* **1997**, *107*, 28−42.
(31) Bodenhausen, G.; Freeman, R.; Niedermeyer, R.; Turner, D. L. *J. Magn. Reson.* **1977**, *26*, 133−164.
(32) Kolbert, A. C.; Griffin, R. G. *Chem. Phys. Lett.* **1990**, *166*, 87−91.
(33) Geen, H.; Bodenhausen, G. *J. Chem. Phys.* **1992**, *97*, 2928−2937.
(34) States, D. J.; Haberkorn, R. A.; Ruben, J. *J. Magn. Reson.* **1982**, *48*, 286−292.
(35) Muller, L.; Ernst, R. R. *Mol. Phys.* **1979**, *38*, 963−992.
(36) McKay, R. A. Personal communication, 1990.
(37) Burum, D. P.; Linder, M.; Ernst, R. R. *J. Magn. Reson.* **1981**, *43*, 463−471.
(38) Raleigh, D. P.; Olejniczak, E. T.; Griffin, R. G. *J. Chem. Phys.* **1988**, *89*, 1333−1350.
(39) Young, D. W.; Tollin, P.; Wilson, H. R. *Acta Crystallogr. B* **1969**, *25*, 1423−1432.
(40) Tran-Dinh, S.; Fermandjian, S.; Sala, E.; Mermet-Bouvier, R.; Cohen, M.; Fromageot, P. *J. Am. Chem. Soc.* **1974**, *96*, 1484−1493.
(41) Sogn, J. A.; Craig, L. C.; Gibbons, W. A. *J. Am. Chem. Soc.* **1974**, *96*, 4694−4696.
(42) Kingsley, P. B. *J. Magn. Reson.* **1994**, *110*, 102−105.
(43) Gregory, D. M.; Wolfe, G. M.; Jarvie, T. P.; Sheils, J. C.; Drobny, G. P. *Mol. Phys.* **1996**, *89*, 1835−1849.
(44) Baldus, M.; Meier, B. H. *J. Magn. Reson., Ser. A* **1996**, *121*, 65−69.
(45) Baldus, M.; Iuliucci, R. J.; Meier, B. H. *J. Am. Chem. Soc.* **1997**, *119*, 1121−1124.
(46) Kumar, A.; Wagner, G.; Ernst, R. R.; Wüthrich, K. *J. Am. Chem. Soc.* **1981**, *103*, 3654−3658.
(47) Simpson, H. J.; Marsh, R. E. *Acta Crystallogr.* **1966**, *20*, 550−555.
(48) Lehmann, M. S.; Koetzle, T. F.; Hamilton, W. C. *J. Am. Chem. Soc.* **1972**, *94*, 2657−2660.
(49) Naito, A.; Ganapathy, S.; Akasaka, K.; McDowell, C. A. *J. Chem. Phys.* **1981**, *74*, 3190−3197.